COMPUTERIZED STABILITY ANALYSIS USING MEASURED INITIAL IMPERFECTIONS

J. Arbocz
Professor of Aircraft Structures
Delft University of Technology, The Netherlands

C.D. Babcock
Professor of Aeronautics
Caltech, California, USA

Abstract

A numerical evaluation of various methods for predicting the buckling load of axially compressed stringer stiffened shells in the presence of initial imperfections was carried out. Both simplified analytical methods and refined computer codes based on finite difference energy formulation (STAGS) were used. The analytical predictions were validated by comparison with the experimentally determined buckling load. As a result of this investigation a method is proposed which makes it possible to take into account both the effect of initial imperfections and the effect of the appropriate boundary conditions.

List of symbols

A_1	- cross-sectional area of stringer
$A_0(x), A_1(x)$	- axial dependence of the radial imperfection, see Eq. (27)
$A_{i0}, A_{k\ell}, B_{k\ell}$	- coefficients of the half-wave cosine Fourier representation, see Eq. (1)
c	- Poisson's effect, $c = \sqrt{3(1-\nu)^2}$
$C_{k\ell}, D_{k\ell}$	- coefficients of the half-wave sine Fourier representation, see Eq. (2)
d_1	- stringer spacing
D_{xx}, D_{xy}, D_{yy}	- effective bending stiffnesses, see Reference [6]
e_1	- distance between centroid of stringer cross-section and middle surface of skin
E	- Young's modulus
f, F	- Airy stress functions
H_{xx}, H_{xy}, H_{yy}	- effective stretching stiffnesses, see Reference [6]
i,k	- number of half-waves in the axial direction
I_{11}	- moment of inertia of stringer cross-section about its centroidal axis
I_{t_1}	- torsional modulus of the stringer cross-section
ℓ	- number of full waves in the circumferential direction
L	- shell length
M_x	- moment resultant
N_{MSS-3}	- perfect shell buckling load using membrane prebuckling analysis and SS-3 boundary condition
N_s	- collapse load of imperfect shell, $N_s = -\lambda_s Et^2/cR$
N_x, N_{xy}, N_y	- stress resultants
q,r,s	- analytical imperfection model parameters, see Eq. (22)
Q_{xx}, Q_{xy}, Q_{yy}	- effective torsional stiffnesses, see Reference [6]
R	- shell radius
t	- shell thickness
u,v,w	- axial, circumferential and radial displacement components, respectively
$w_0(x), w_1(x), W$	- radial displacement, positive outward, see Eq. (28)
$\bar{w}, \bar{W}$	- radial imperfection from perfect cylinder
$\bar{W}_{i0}, \bar{W}_{k\ell}, \bar{W}'_{k\ell}$	- initial imperfection harmonics, see Eq. (20)
x,y	- axial and circumferential coordinates on the middle surface of the shell, respectively
$\bar{x}, \bar{y}$	- nondimensional coordinates, $\bar{x} = \pi x/R$, $\bar{y} = y/R$
$\bar{X}_A, \bar{X}$	- analytical imperfection model parameters, see Eq. (22)
Z	- Batdorf's shell parameter, $Z = (L^2/Rt)\sqrt{1-\nu^2}$
α_k, β_ℓ	- mode shape parameters, see Reference [6]
$\bar{\gamma}_{D,k,\ell,\ldots}$	- nondimensional stiffener parameters, see Reference [6]
θ	- circumferential coordinate, $\theta = y/R$
λ	- nondimensional loading parameter, $\lambda = cRN_x/Et^2$
λ_{ci}	- classical axisymmetric buckling load
$\lambda_{ck\ell}$	- classical asymmetric buckling load, see Eq. (10)
λ_s	- collapse load of imperfect shell
ν	- Poisson's ratio
ξ_1, ξ_2	- axisymmetric and asymmetric response amplitudes, respectively
$\bar{\xi}_1, \bar{\xi}_2$	- axisymmetric and asymmetric imperfection amplitudes, respectively
$\hat{\xi}$	- equivalent initial imperfection amplitude
ρ	- nondimensional loading parameter, $\rho = N_x/N_{MSS-3}$

1. Introduction

The stability calculations of axially compressed cylindrical shells continue as one of the most difficult and most challenging of all the structural analysis problems. To illustrate this fact, in figure 1[1] the available experimental results for axially compressed stringer stiffened shells have been plotted as a function of Batdorf's Z parameter. The experimental buckling loads have been normalized by the theoretical buckling loads computed from a linearized small deflection theory using SS-3 ($N_x = v = w = M_x = 0$) boundary conditions. The effects of in-plane boundary conditions[2] and of initial imperfections[3] have been accepted as the main cause for the wide experimental scatter seen in this figure. Despite this recognition the incorporation of these factors into a rational

design procedure has not been accomplished as yet. Actual shell structures are still being designed in the old-fashioned way by using an empirical knock-down factor such that, when it is multiplied by the classical buckling load a lower bound to all the available experimental data for the given configuration is obtained. If, however, all the effort and money spent in recent years on research in shell stability and on developing sophisticated computer codes is to become beneficial to all the practicing structural engineers, then it is necessary to combine the latest scientific findings into a shell design approach which accounts for the effects of both the initial imperfections and the correct experimental boundary conditions.

Since it is felt that the mathematical and experimental tools for handling axially compressed stringer stiffened shells have been sufficiently developed, therefore in this paper a concentrated effort is made toward finding a method (or methods) which will reliably and economically predict the buckling loads of such shells. It is considered especially desirable to ascertain whether or not one can calculate the buckling load from measured (or predicted) initial imperfections by using one of the specialized or simplified analytical methods [3,4,5,6], or whether it is necessary to resort to one of the large multipurpose computer codes such as STAGS[7] for satisfactory solution. In all the examples presented the laboratory scale shell AS-2, tested in 1970 at Caltech[8] is used, since for this shell complete surface scans made before and during the buckling test are available. Finally the buckling loads calculated by the different methods are compared with the experimental buckling load.

2. Experimental program

For a detailed description of the test program dealing with buckling tests of axially compressed machined integrally stiffened cylindrical shells the reader is referred to Reference [8]. Here only the principal results are summarized which are needed for the analytical and numerical buckling load calculations reported in this paper.

The geometry of the stringer stiffened shell AS-2 is shown in Fig. 2. The geometric and material properties are summarized in Table 1. The buckling test was carried out in a controlled end displacement type testing machine with an attached scanning device built around a noncontacting capacitance type pick-up. After the shell was installed in the testing machine, the pick-up calibration was performed and an initial scan was taken. Then the axial load was increased in small increments and the scanning repeated until buckling occurred. Data reduction was done using the procedure described in detail in Reference [5]. The cards containing the measured deviations from the perfect shell at zero axial load were used to prepare the 3-dimensional plot of the initial imperfections shown in Fig. 3 by offsetting the origin of the successive circumferential scans by the proper amount along both the x- and y-axes.

The coefficients of the following double Fourier series

$$\bar{w}(x,y) = t\bar{W}(x,y) = t \sum_{i=0}^{N} A_{io} \cos \frac{i\pi x}{L} + t \sum_{k,\ell=0}^{N} \cos \frac{k\pi x}{L} \left(A_{k\ell} \cos \frac{\ell y}{R} + B_{k\ell} \sin \frac{\ell y}{R} \right) \quad (1)$$

and

$$\bar{w}(x,y) = t\bar{W}(x,y) = t \sum_{k,\ell=0}^{N} \sin \frac{k\pi x}{L} \cdot \left(C_{k\ell} \cos \frac{\ell y}{R} + D_{k\ell} \sin \frac{\ell y}{R} \right) \quad (2)$$

which were computed numerically, are displayed in Tables 2 and 3. For clearer representation any amplitude smaller than 0.005 t (= 0.0001 cm) was replaced by zero. It should be noticed that for the stringer stiffened shell AS-2 the amplitudes of the axisymmetric imperfections ($\ell = 0$) are insignificant.

The available experimental data will be used with different analytical methods. Thereby initial imperfection representations of increasing complexity will be used.

3. Analytical results

Since the pioneering works of Donnell and Wan[9] and Koiter[10] many different approximate methods [4,11,12] have been proposed to take into account the effect of different types of initial imperfections when calculating the buckling loads of axially compressed cylindrical shells. Before briefly summarizing the most important ones let us first consider the mathematical formulation of the stability problem.

Assuming that the stiffener properties are "smeared out" and using the component of displacement W normal to the shell midsurface (positive outward) and an Airy stress function F (with $N_x = F_{,yy}$, $N_y = F_{,xx}$ and $N_{xy} = -F_{,xy}$) as the dependent variables, then the governing equations can be written as[13]

$$L_H(F) - L_Q(W) = \frac{1}{R} W_{,xx} - \frac{1}{2} L_{NL}(W, W + 2\bar{W}) \quad (3)$$

$$L_Q(F) + L_D(W) = -\frac{1}{R} F_{,xx} + L_{NL}(F, W + \bar{W}) \quad (4)$$

where the linear operators are

$$\begin{aligned} L_H(\,) &= H_{xx}(\,)_{,xxxx} + H_{xy}(\,)_{,xxyy} + H_{yy}(\,)_{,yyyy} \\ L_Q(\,) &= Q_{xx}(\,)_{,xxxx} + Q_{xy}(\,)_{,xxyy} + Q_{yy}(\,)_{,yyyy} \\ L_D(\,) &= D_{xx}(\,)_{,xxxx} + D_{xy}(\,)_{,xxyy} + D_{yy}(\,)_{,yyyy} \end{aligned} \quad (5)$$

and the nonlinear operator is

$$L_{NL}(S,T) = S_{,xx}\, T_{,yy} - 2S_{,xy}\, T_{,xy} + S_{,yy}\, T_{,xx} \quad (6)$$

Subscripts following a comma denote partial differentiation. The parameters D_{xx}, H_{xx}, Q_{xx}, D_{xy}, ..., etc., are defined in Reference [6].

These equations, together with the appropriate boundary conditions, govern the behaviour of circular cylindrical shells

1. In the prebuckling stress and deformation state.

2. At the limit point or bifurcation point (if there is one).
3. In the postbuckling stress and deformation state.

When discussing the effects of the different types of imperfections it is customary to compare the buckling loads of the imperfect shells to the buckling load of the perfect shell.

3.1. Classical linearized small-deflection theory for a perfect shell[6]

For a perfect shell, $\bar{W} = 0$. If one assumes a "membrane" prebuckling solution and lets $\hat{W}, \hat{F}$ represent small perturbations at the bifurcation point, then

$$W = \frac{\nu}{c} \lambda t \frac{\bar{H}_{xx}}{1+\mu_1} + \hat{W} \tag{7}$$

$$F = -\frac{Et^2}{c} \frac{\lambda}{2} \frac{y^2}{R^2} + \hat{F} \tag{8}$$

Direct substitution into Eqs. (3) and (4) and deletion of products of the perturbation quantities yields a set of linearized stability equations in $\hat{W}$, $\hat{F}$[6]. These equations admit solutions of the form

$$\hat{W} = A \sin \frac{k\pi x}{L} \cos \frac{\ell y}{R}$$

$$\hat{F} = B \sin \frac{k\pi x}{L} \cos \frac{\ell y}{R} \tag{9}$$

leading to a standard eigenvalue problem with eigenvalues

$$\lambda_{c_{k\ell}} = \frac{1}{2} \left\{ \frac{\bar{\gamma}_{D,k,\ell}}{\alpha_k^2} + \frac{(\bar{\gamma}_{Q,k,\ell} + \alpha_k^2)^2}{\alpha_k^2 \bar{\gamma}_{H,k,\ell}} \right\} \tag{10}$$

where

$$N_{x_{k\ell}} = -\lambda_{c_{k\ell}} \frac{E}{c} \frac{t^2}{R} \tag{11}$$

and the parameters $\bar{\gamma}_{D,k,\ell}$, $\bar{\gamma}_{Q,k,\ell}$, ..., etc., are defined in Reference [6]. The variation of the nondimensional classical buckling load ρ as a function of the axial half wave number k and the circumferential wave number ℓ is shown in Fig. 4. For the stringer stiffened shell AS-2 the lowest eigenvalue ($\rho = 1.0$) is single valued and is associated with an asymmetric mode that has one half wave in the axial direction and 10 waves in the circumferential direction. Also, as can be seen from Fig. 4 there are only three modes with eigenvalues less than 1.10 (within 10% of the lowest eigenvalue $\rho = 1.0$). As a matter of fact there are only a few modes with eigenvalues less than 1.50. Also it should be mentioned that the eigenfunctions satisfy the classical simply supported boundary conditions ($N_x = v = w = M_x = 0$). The normalizing factor in this case is $N_{M_{SS-3}} = -229.8$ N/cm (= -131.2 LB/IN).

If one assumes that the imperfections of the real shell can be represented by some "equivalent" axisymmetric imperfection then the governing equations (3) and (4) can be solved quite readily.

3.2. Effect of axisymmetric imperfection[11]

Suppose at the bifurcation point

$$W = W^* + \hat{W} \; ; \quad F = F^* + \hat{F} \tag{12}$$

where W^*, F^* represent the prebuckling solution and $\hat{W}$, $\hat{F}$ are small preturbations at buckling. Direct substitution into Eqs. (3) and (4) and deletion of squares and higher order terms of the perturbation quantities yields a set of nonlinear governing equations for the prebuckling quantities[6] and a set of linearized stability equations governing the perturbation quantities[6].

For a given axisymmetric imperfection the prebuckling problem is also axisymmetric and a particular solution of the governing ordinary differential equations is obtained in a straight forward manner. If as a first approximation the effect of boundary conditions is neglected then one does not have to include the complementary solutions.

Assuming separable solutions the linearized stability equations can be solved as follows. First a particular solution of the compatibility equation is obtained for $\hat{F}$. This guarantees that a kinematically admissible displacement field is associated with an approximate solution of the equilibrium equation. Then a straight forward application of Galerkin's procedure yields a characteristic equation in the form of a cubic polynomial in the eigenvalue parameter λ[4,6,11].

It is known that from an axisymmetric prebuckling state bifurcation may occur into either a symmetric or an antisymmetric mode. For shell AS-2 all the cases investigated has a symmetric prebuckling state. For the case shown in Fig. 5 the initial imperfection consisted of a full wave cosine mode pointing inward at the middle of the shell. This resulted in a prebuckling state dominated by a full wave cosine axisymmetric mode with the radial deflection pointing inward at the midplane of the shell. Bifurcation occurs into an, in the axial direction symmetric mode consisting of a half wave sine in the axial and 10 full waves in the circumferential direction. For increasing initial imperfection amplitudes $\bar{\xi}_1$ bifurcation occurs at ever smaller values of the axial load parameter ρ. Thus, for instance, for $\bar{\xi}_1 = 1.0$ $\rho_{BIF} = 0.53$.

The use of the results of this analysis, as represented by Fig. 5 with the experimentally measured initial imperfection harmonics of Tables 2 and 3 yields "knock-down" factors of practically 1.0 for shell AS-2. This failure to predict any noticeable decrease of the buckling load is due to the fact that the amplitudes of the axisymmetric harmonics of interest (k = 2 for the half-wave cosine) are very small ($A_{2,0} = 0.005$). If one computes the RMS (root mean square) value of the measured axisymmetric distribution (see Reference [14] for details) and uses it as the amplitude of the required harmonic, even then no significant "knock-down" factors can be found by this approach.

If one accepts the "WHITE NOISE" assumption that all initial imperfection components have the same amplitude, then it follows that the largest knock-down factor will be caused by that component which corresponds to the buckling mode of the lowest (or classical) buckling load. For the

stringer stiffened shell AS-2 the lowest bucling load is associated with an asymmetric bucling mode.

3.3. Effect of asymmetric imperfection (b-factor method)[4]

Koiter has shown that the buckling load of an imperfect shell λ_s (defined as the maximum load the structure can support prior to buckling) is related to the imperfection amplitude $\bar{\xi}_2$ and the postbuckling coefficient b by

$$\left(1-\frac{\lambda_s}{\lambda_{c_{k\ell}}}\right)^{3/2} = \frac{3}{2}\sqrt{3}\sqrt{-b}\,\frac{\lambda_s}{\lambda_{c_{k\ell}}}\,|\bar{\xi}_2| \quad \text{for } b<0 \qquad (13)$$

if the lowest buckling load is single valued and the associated buckling mode is asymmetric. Imperfection sensitive structures are characterized by negative values of b.

To calculate the postbuckling coefficient b for the case where a unique buckling mode $W^{(1)}$, $F^{(1)}$ corresponds to the classical buckling load $\lambda_{c_{k\ell}}$, one begins by assuming a solution valid in the initial postbuckling regime in the form of an asymptotic expansion

$$\begin{aligned} W &= \lambda W^{(0)} + \xi W^{(1)} + \xi^2 W^{(2)} + \ldots \\ F &= \lambda F^{(0)} + \xi F^{(1)} + \xi^2 F^{(2)} + \ldots \\ \frac{\lambda}{\lambda_{c_{k\ell}}} &= 1 + a\xi + b\xi^2 + \ldots \end{aligned} \qquad (14)$$

A formal substitution of this expansion into the nonlinear Donnell type equations (3) and (4) for a perfect shell ($\bar{W} = 0$) generates a sequence of linear equations for the functions appearing in the expansion. General expressions for the post-buckling coefficients a and b have been derived by Budiansky and Hutchinson[15].

As mentioned before the stringer stiffened shell AS-2 has a single valued lowest buckling load with an asymmetric buckling mode

$$W^{(1)} = \hat{C}_{k\ell}\,\sin\frac{k\pi x}{L}\cos\frac{\ell y}{R} \qquad (15)$$

In this case the first post-buckling coefficient "a" is identically zero and the b-factor method is applicable. If one neglects prebuckling deformations, then the classical membrane solution satisfies the governing equations of the 0^{th} order state. The set of equations for $W^{(1)}$, $F^{(1)}$ is just the classical eigenvalue problem discussed earlier. Finally for $W^{(2)}$, $F^{(2)}$ one must solve a set of linear, inhomogeneous partial differential equations whose forcing functions involve the $W^{(1)}$, $F^{(1)}$ terms. These equations admit separable solutions whose unknown coefficients are readily determined by Galerkin's procedure[6]. Finally the post-buckling coefficient b is calculated by evaluating the integrals indicated[4].

It should be remarked here that the b-factor is actually a property of the perfect shell. Once the b-factor is calculated for a given shell geometry then a plot like the one in Fig. 6 can be plotted. This figure shows the amount of axial load the shell AS-2 will carry as a function of the amplitude $\bar{\xi}_2$ of an asymmetric imperfection consisting of a half wave sine in the axial direction and 10 full waves in the circumferential direction. For instance, for $\bar{\xi}_2 = 1.0$, $\rho_s = 0.584$. The line with the arrows indicates the effect of the measured initial imperfections, thus for

$$\hat{\xi} = \sqrt{C_{1,10}^2 + D_{1,10}^2} = 0.054\,, \quad \rho_s = 0.93$$

Experimental evidence, like the initial imperfection plot for shell AS-2 shown in Fig. 3, seems to indicate that in a given shell both axisymmetric and asymmetric imperfection components are present

3.4. Effect of axisymmetric and asymmetric imperfections (2-mode solution)[16]

If one assumes that the initial radial imperfection is given by

$$\frac{\bar{W}}{t} = \bar{\xi}_1\cos\frac{i\pi x}{L} + \bar{\xi}_2\sin\frac{k\pi x}{L}\cos\frac{\ell y}{R} \qquad (16)$$

then any equilibrium state of the axially loaded cylinder can be represented by

$$\begin{aligned} W &= \frac{\nu}{c}t\lambda\,\frac{\bar{H}_{xx}}{1+\mu_1} + t\xi_1\cos\frac{i\pi x}{L} + t\xi_2\sin\frac{k\pi x}{L}\cos\frac{\ell y}{R} \\ F &= -\frac{Et^2}{c}\frac{y^2}{2R}\lambda + f \end{aligned} \qquad (17)$$

An approximate solution of the nonlinear Donnell-type equations is obtained as follows. First, the compatibility equation (3) is solved exactly for the stress function f in terms of the assumed radial displacement W and the measured imperfection $\bar{W}$. In this solution only the effect of initial imperfections on the buckling load is of interest. Hence, only a particular solution of Eq. (3) needs to be considered. Second, the equilibrium equation (4) is solved approximately by substituting therein F, W and $\bar{W}$, and then applying Galerkin's procedure. This procedure yields the following set of nonlinear algebraic equations in terms of the unknown amplitudes ξ_1 and ξ_2:

$$\begin{aligned} &(\lambda c_i - \lambda)\,\xi_1 - \underline{C_1(\tfrac{1}{2}\xi_2^2 + \xi_2\bar{\xi}_2) - C_2(\xi_2+\bar{\xi}_2)\,\xi_2} \\ &\qquad + C_2[(\xi_1+\bar{\xi}_1)\,\xi_2 + \xi_1\bar{\xi}_2](\xi_2+\bar{\xi}_2) = \lambda\bar{\xi}_1 \end{aligned} \qquad (18)$$

$$\begin{aligned} &(\lambda c_{k\ell}-\lambda)\,\xi_2 - \underline{C_3[2(\xi_1+\bar{\xi}_1)\,\xi_2+\xi_1\bar{\xi}_2] - C_4(\xi_2+\bar{\xi}_2)\,\xi_1} \\ &\qquad + (C_9+C_{10})(\tfrac{1}{2}\xi_2^2+\xi_2\bar{\xi}_2)\,(\xi_2+\bar{\xi}_2) \\ &\qquad + C_{11}[(\xi_1+\bar{\xi}_1)\,\xi_2 + \xi_1\bar{\xi}_2](\xi_1+\bar{\xi}_1) = \lambda\bar{\xi}_2 \end{aligned}$$

The coefficients C_1 through C_{11} are listed in Reference [6]. The underscored quadratic coupling terms vanish identically unless the condition i = 2k

is satisfied. It has been shown in Reference [17] that the cubic terms should not be neglected. Solution of these nonlinear equations yields the equilibrium configuration of the finite shell as a function of λ shown in Fig. 7. If λ attains a maximum as the compressive axial load is increased, then by definition this value of $\lambda = \lambda_s$ at the limit point is associated with the buckling load. Working with different combinations of harmonics it is possible to locate the "pair of critical modal components", defined as that combination of one axisymmetric and one asymmetric component that would yield the lowest value for λ_s for identical initial amplitudes.

For shell AS-2 this critical pair consists of the asymmetric classical buckling mode (1,10) and the axisymmetric mode (2,0), which satisfies the quadratic coupling condition i = 2k. Here the notation (2,0) stands for an axisymmetric cosine mode with two half waves in the axial direction, whereas (1,10) denotes an asymmetric mode with a half wave sine in the axial and 10 full waves in the circumferential direction. For an initial imperfection consisting of the pair of critical modal components Fig. 8 shows the amount of axial load shell AS-2 will carry as a function of the indicated imperfection amplitudes. Curves for constant values of the axisymmetric imperfection $\bar{\xi}_1$ and for increasing values of the asymmetric imperfection $\bar{\xi}_2$ are plotted. The line with the arrows indicates the effect of the measured initial imperfections when this model is used ($\rho_s = 0.91$).

In order to incorporate any desired detail of themeasured initial imperfections and to model the nonlinear interaction between certain modal components one must resort to doube Fourier representations.

3.5. Effect of general imperfections (multimode solution)[3,12]

Initially, by Newton's method of quasilinearization the nonlinear Donnell type imperfect shell equations (3) and (4) are reduced to a set of linear partial differential equations for determining the correction terms δF, δW. If one represents the initial imperfections by

$$\frac{\bar{W}}{t} = \sum_{i=1}^{N_1} \bar{W}_{io} \cos\frac{i\pi x}{L} + \sum_{k,\ell=1}^{N_2} \bar{W}_{k\ell} \sin\frac{k\pi x}{L} \cos\frac{\ell y}{R} + \sum_{k,\ell=1}^{N_3} \bar{W}'_{k\ell} \sin\frac{k\pi x}{L} \sin\frac{\ell y}{R} \tag{20}$$

then these equations admit separable solutions[3]. The unknown coefficients are determined by Galerkin's procedure yielding a set of linear algebraic equations in terms of the unknown correction terms. In matrix notation

$$\begin{aligned} [A]\{\delta F\} + [B]\{\delta W\} &= -\{E^{(1)}\} \\ [C]\{\delta F\} + [D]\{\delta W\} &= -\{E^{(2)}\} \end{aligned} \tag{21}$$

To obtain the buckling load for a given imperfect cylindrical shell one begins by making an initial guess for $\{W\}$ and $\{F\}$ at a small initial load level λ. Iteration is then carried out until the correction vectors are smaller than some preselected value. The converged solutions then are used as the initial guess at the next higher axial load level $\lambda + \Delta\lambda$. The entire process is repeated for increasing values of the axial load parameter λ. Close to the limit point one then switches to increments in the nonlinear part of the end-shortening $\Delta\delta_{NL}$, which makes it possible to integrate around the limit point. By definition, the value of the loading parameter λ corresponding to the limit point will be the theoretical buckling load.

When applying the Multimode Analysis to the shell AS-2 the amplitudes of the harmonic components could be selected from the values given in Tables 2 and 3. However, when observing such data displayed on a log-log basis[18] it is evident that the imperfection amplitude coefficients can be approximated by straight lines as follows:

$$\bar{W}_{io} = \frac{\bar{X}_A}{i^q} \; ; \quad \bar{W}_{k\ell} = \frac{\bar{X}}{k^r \ell^s} \tag{22}$$

where

$\bar{W}_{io}$ = amplitude of the i^{th} axisymmetric Fourier cosine harmonic,
$\bar{W}_{k\ell}$ = amplitude of the k,ℓ^{th} asymmetric Fourier sine harmonic,
$\bar{X}_A$, $\bar{X}$, q, r, s = coefficients obtained by least square fitting the measured data

This imperfection model has several advantages. In the first place, the correlation studies carried out with shells other than AS-2 required in some cases imperfection amplitudes at wave numbers that were not measured. This was due to the fact that the early experimental data spacing was not sufficiently close to resolve all the harmonic amplitudes of interest. Therefore, the imperfection model was fitted over the wave numbers actually measured and then the amplitudes of the harmonics of interest could be obtained by extrapolation. The accuracy of this procedure is as yet unknown.

Secondly, the imperfection model fitting is a numerical smoothing operation of the experimental data. It is felt that such an operation is desirable due to the experimental scatter experienced in obtaining the imperfection measurements.

Thirdly, it is highly desirable to have an imperfection model that represents a class of shells manufactured by a given process. Utilizing this characteristic imperfection model the multimode analysis can be used to carry out imperfection sensitivity calculations, enabling the designer to choose a more realistic "knock-down factor" for the shell well before the detailed shell imperfections are available. The parameters of the imperfection model used for shell AS-2 are given in Table 4.

Since the number of modes that can be included in the analysis is limited by practical considerations, the question arises: "How does one decide which of the many harmonic components are important and hence should be included in the analysis?" Previous studies with axially compressed cylindrical [3,6] have shown that imperfections dominate the behaviour of the shell if at or close to the lowest eigenvalue the corresponding modes have significant

initial amplitudes. Conversaly, imperfections do not play such a significant role if at or close to the lowest eigenvalue the corresponding modes have no significant initial amplitudes. Hence one must always consider the distribution of the eigenvalues for a given shell and the amplitudes of the Fourier coefficients of the measured initial imperfections simultaneously.

The normalized buckling loads for shell AS-2 are shown in Fig. 4. As mentioned before these eigenvalues were computed using a membrane prebuckling solution with the classical simply supported boundary conditions ($N_x = v = w = M_x = 0$), and they are normalized by the lowest buckling load $N_{MSS-3} = -229.8$ N/cm (= -131.2 LB/IN). The lowest eigenvalue ($\rho = 1.0$) is single valued and is associated with an asymmetric buckling mode with one half-wave in the axial direction and 10 full waves in the circumferential direction. Comparing the distribution of eigenvalues with the initial amplitudes of the corresponding eigenfunctions (or Fourier coefficients) shown in Table 3, one expects that, since there are significant initial imperfections close to the (1,10) mode, the buckling load of the real (imperfect) shell AS-2 will be noticeably lower than the corresponding classical value obtained for the perfect shell.

Results of buckling load calculations for shell AS-2 using the multimode analysis are summarized in Table 5. In this table the notation (2,0) denotes a cosine axisymmetric mode with two half-waves in the axial direction, whereas (1,10) denotes an asymmetric mode with a single half-wave sine in the axial direction and 10 full waves in the circumferential direction. Comparing the result of the 2-mode solution with that of the 4-mode solution it is evident that the additional short wavelength modes have only an insignificant effect. The reason for this becomes immediately evident if one considers the distribution of eigenvalues for the shell AS-2 shown in Fig. 4. Only the eigenvalues of a few asymmetric modes with long wavelength in the axial direction are close to the lowest eigenvalue, which in this case is asymmetric. Coupling of these modes results in a significant decrease in the predicted buckling load. The in this case insignificant effect of the short wave-length axial modes is further illustrated by the fact that after the elimination of these modes from the 14-modes imperfection model one obtains a buckling load of $\rho_s = 0.825$ (7-modes solution), only slightly higher than the value of $\rho_s = 0.824$ which the 14-modes solution itself predicts.

In selecting additional modes, besides the magnitude of the initial imperfection and the relative size of the corresponding eigenvalue, special attention must be given to the satisfaction of the axial and circumferential coupling conditions. It has been shown[19] that for the degenerate case of one axisymmetric (i,o) and one asymmetric mode (k,ℓ) there is a single coupling relation i = 2k. Furthermore, it has been found that coupling between three asymmetric modes with wave-numbers (k,ℓ), (m,n) and (p,q) will occur if the relations k + m + p = odd integer and $q = |\ell + n|$ hold. This implies that if the coupling conditions are satisfied, then the resulting buckling load of the shell will be lower than the buckling load which is predicted with each mode considered separately.

The results of Table 5 indicate that the inclusion of properly chosen additional modes leads to decreasing buckling loads. That is, in going from a 2-modes to a 7-modes solution, the addition of 5 new modes results in a 8% decrease of the predicted buckling load. For the 14-modes solution, the inclusion of seven additional modes produces only a further 0.1% decrease. This behaviour suggests that there is a point beyond which the addition of more modes will not necessarily result in a further significant decrease of the predicted buckling load. Hence the value of $\rho_s = 0.82$ will be used as the estimated lower limit.

To calculate the theoretical buckling load of the real (imperfect) externally stringer stiffened shell AS-2 one must also include the effects of the in-plane boundary conditions. This can be done by the formula proposed in Reference [20]. In the experimental set-up the ends of the shell were cast in Cerrolow, a low melting point alloy[8]. If one assumes that this corresponds to a C-4 boundary condition ($u = v = w = w_{,x} = 0$) then

$$N_{S_{C-4}} = \rho_s N_{M_{C-4}} = (0.82)(-320.8) = -263.1 \text{ N/cm}$$
$$= (0.82)(-183.2) = -150.22 \text{ LB/IN} \quad (23)$$

If, however, one claims that the experimental boundary conditions are C-3 ($N_x = v = w = w_{,x} = 0$) then

$$N_{S_{C-3}} = \rho_s N_{M_{C-3}} = (0.82)(-256.9) = -210.7 \text{ N/cm}$$
$$= (0.82)(-146.7) = -120.29 \text{ LB/IN} \quad (24)$$

In the actual test the shell AS-2 buckled at $N_{EXP} = -226.4$ N/cm (= -129.3 LB/IN)[8]. Thus $N_{S_{C-4}} = -263.1$ N/cm and $N_{S_{C-3}} = -210.7$ N/cm represent an upper and a lower bound to the experimental buckling load. Still the discrepancy between the predicted and the experimental buckling loads needs an explanation. To this effect especially the question of the correct experimental boundary conditions and the adequacy of the representation of the measured initial imperfections by the proposed imperfection models will be investigated.

4. Numerical results

Since the purpose of the work reported in this paper was to investigate the capability of different methods available for predicting the buckling of stiffened circular cylinders in the presence of imperfections, therefore it was decided to use the existing computer codes BOSOR[21], SRA[22] and STAGS[7] for carrying out the investigations reported in the following sections.

4.1. Study of the experimental boundary conditions

In calculating the buckling loads of cylindrical shells, particularly axially stiffened shells, it is important to carefully consider the actual boundary conditions of the shell. The important parameters appear to be the axial stiffness which causes the difference between SS-3 and SS-4 (see Table 6 for definition of boundary conditions) or C-3 and C-4, and the end ring torsional stiffness which causes the difference between SS-3 and C-3 or SS-4 and C-4. It is usually assumed that the end support structure is rigid enough to suppress

the radial displacement w and the circumferential displacement v.

Singer and Rosen[23,24] have studied the end support fixity problem. This work has utilized an experimental determination of the natural frequencies of the test shell to predict the appropriate stiffness parameters. The experiments are conducted while the shell is under some axial load to insure a good contact between shell and end fixture. The published results[23,24] indicate that the typical experimental "clamped" boundary condition is somewhat less than fully clamped (C-4). However, it is not clear if this is an axial restraint problem or one of torsional restraint, although Singer and Rosen assume it to be the torsional restraint for the experimental end fixity in question. From their results on 4 "clamped" shells (RO-31, RO-33, RO-45, RO-46) they conclude that the theoretical buckling load using the experimental boundary conditions would be reduced 2-9% from the fully clamped (C-4) boundary condition. This reduction correlates well with the nondimensional stiffener moment of inertia (I_{11}/d_1t^3), with the lightly stiffened shells having a smaller reduction from the C-4 boundary condition. Compared to the stiffened shells tested by Singer and Rosen[23,24] shell AS-2[8] falls near the lower end of the stiffener parameters. Although the end fixture arrangement is quite different, one would expect about a 2-3% reduction from the buckling load with C-4 boundary condition.

In order to further confirm this conclusion, a theoretical investigation was undertaken using the SRA-code[22]. The actual test setup consists of 3 cylindrical pieces in series which are bonded to the end plates of the testing machine[8]. The first is a heavy steel cylinder which is used as a spacer. The test shell is attached to this spacer and in turn is supported on the other end by an end ring attached to another short cylinder serving as a load cell. The load is determined by 24 strain gages spaced around the circumference of the load cell cylinder. A drawing of the arrangement and the computer model parameters used in SRA are shown in Fig. 9.

With this model the buckling load was computed using the branch of SRA which includes nonlinear prebuckling deformation. This program incorporates an automatic choice of the integration steps which guarantees that the convergence criterion set by the user is satisfied. The results showed that the buckling load of the complete model was -316.6 N/cm (= -180.8 LB/IN) and that the shell buckled into 14 full waves around the circumference and 2 half waves along the length. The prebuckling displacement and the buckling mode are shown in Fig. 10. As can be seen from this figure, the ends of the shell do not undergo much displacement either before buckling or during buckling.

In order to assess the influence of the experimental end fixity on the buckling load, the buckling load with idealized C-4 boundary condition must be determined. Reference [3] reports this buckling load as 316.8 N/cm (= 180.9 LB/IN) using the same SRA code. Comparing the two values the buckling load using experimental boundary conditions is 0.06% lower. The conclusion, therefore, is reached that the experimental setup as used in the buckling test of shell AS-2[8] very nearly approaches the idealized fully clamped (C-4) boundary condition. Thus in the remainder of this work this idealized (C-4) boundary condition will be used for the computer models.

Next the collapse analysis capabilities of the STAGS-A code were tested by comparison with existing solutions obtained by a different analysis technique. It should be mentioned here that all the results discussed in the following sections were obtained with a fully double precision version of STAGS-A, which is operational on the IBM370-158 at the Delft University of Technology. Thus the difference in single precision word length between the CDC and the IBM computers no longer can cause any problems.

4.2. Collapse analysis with idealized imperfections

Rather than writing a special subroutine WIMP for each imperfection model to be tested, it was decided to write a general subroutine WIMP which allows the input of imperfection data on cards. For this the initial imperfection is represented by the following double Fourier series:

$$\bar{W} = t \sum_{i=1}^{N_1} \bar{W}_{io} \cos i\bar{x} + t \sum_{k,\ell=1}^{N_2} \bar{W}_{k\ell} \sin k\bar{x} \cos \ell\bar{y} + t \sum_{k,\ell=1}^{N_3} \bar{W}'_{k\ell} \sin k\bar{x} \sin \ell\bar{y} \tag{25}$$

where $\bar{x} = \pi x/L$, $\bar{y} = y/R$. This is the same representation that is used for the Multimode Analysis [3].

To check out this subroutine and to test the collapse analysis capabilities of the STAGS-A code the following idealized imperfection model is used

$$\frac{\bar{W}}{t} = 0.01 \cos 2\bar{x} + 0.50 \sin \bar{x} \cos \ell\bar{y} \tag{26}$$

where with the C-3 boundary conditions $\ell = 11$, whereas with C-4 $\ell = 13$. In the STAGS-A code positive radial displacement is outward. For the test runs the stringer stiffened shell XS-1 is employed. This shell has exactly the same dimensions as the shell AS-2, except that its length is 10.16 cm (= 4.0 IN) instead of 13.97 (= 5.5 IN). For comparison there are results available, which were obtained by different analysis technique for C-3 and C-4 boundary conditions.

This so-called Extended Analysis[20] solves the imperfect shell collapse problem by making an assumption on the circumferential dependence of the initial imperfection and the response variables. The resulting nonlinear two-point boundary value problem is solved using a multi segment shooting technique. This leaves complete freedom in the axial dependence of the shell deflections and stresses but restricts their circumferential dependence. For example, for an initial imperfection of the form

$$\bar{W}(x,\theta) = tA_o(x) + tA_1(x) \cos \ell\theta \tag{27}$$

where $\theta = y/R$ and $A_o(x)$, $A_1(x)$ are known functions of x, the radial displacement W is expressed as follows:

$$W(x,\theta) = tw_o(x) + tw_1(x) \cos \ell\theta \tag{28}$$

where $w_o(x)$, $w_1(x)$ are unknown functions of x.

The STAGS code, on the other hand, does not restrict the variation in either the axial or circumferential directions. It is obvious, however, that if the initial imperfection is periodic with period $2\pi/\ell$ radians then the STAGS analysis can be accomplished using only a small segment of the complete shell. For the present analysis the initial imperfection is also symmetric in the axial direction about the center of the shell. Thus a further reduction in the segment used for the analysis is possible with the recognition, that the response will be symmetric also about the center of the segment isolated by periodicity. This allows the analysis to be completed in a sector shown in Figure 11.

From the results of the study of the experimental boundary conditions it was concluded that they could be adequately modeled by the idealized C-4 boundary condition. This presents one problem, however, since the C-4 boundary condition on the buckling mode suppresses the axial displacement u at both ends of the shell, thereby preventing any load from being applied to the shell. This can be circumvented by applying an axial displacement to one end of the shell while holding the other end fixed. Unfortunately, in a nonlinear imperfect shell analysis, the axial displacement is a difficult quantity to estimate beforehand, while the axial collapse load can be roughly guessed from prior analytical results.

This problem was dealt with by initially running the imperfect shell with the idealized C-3 boundary condition at the loaded end. The average u values at the loaded end then can be used to estimate the axial displacements that should be applied in the case with the C-4 boundary condition. The results of the STAGS-S run with C-3 boundary conditions at the loaded end were validated by comparing them to similar results obtained by the Extended Analysis[20]. Figure 12 shows the maximum displacement as a function of axial load. This maximum displacement is the radial displacement W at $x = L/2$ and $\theta = 120/11 = 16.36^o$. Each point indicated by a circle represents a nonlinear STAGS run. Above the last point the solution would not converge at even a very small load increment. It was assumed that this represented the collapse load which corresponds to $\rho_s = 0.607$. The load parameter ρ has been nondimensionalized by the perfect shell buckling load, which for the shell XS-1 is -283.0 N/cm ($= -161.6$ LB/IN) for the C-3 boundary condition[3]. The Extended Analysis[20] results are given by the solid curve. Its limit point occurs at $\rho_s = 0.635$, which is very close to the value obtained by STAGS.
It seems reasonable that STAGS produces a lower result since it used a coarser mesh. In the Extended Analysis the integration step sizes are chosen automatically such that the specified local truncation error tolerance is satisfied.

The shapes of the collapse modes obtained by the two analyses are shown in Fig. 13. The points indicated by circles represent the STAGS analysis and the solid lines are from Reference [20]. A comparison at equal loads becomes impossible near the collapse point since the Extended Analysis goes to higher loads than the STAGS results. It is apparent from Fig. 13a, and it has been shown in Reference [25] that if the comparison is made at equal maximum amplitudes then for the axial variation of the radial displacement at $\theta = 16.36^o$ the results are identical to within plotting accuracy. For the circumferential variation of the radial displacement at $x = L/2$, Fig. 13b, minor differences will remain also in that case. Considering the completely different analysis techniques the agreement is quite good.

Next the modeling of the C-4 boundary condition, by applying a given axial displacement at the loaded end, was validated by comparison with an Extended Analysis result[20]. The radial displacement W at $x = L/2$ and $\theta = 180/13 = 13.85^o$ (the maximum displacement W/t) as a function of the load is shown in Fig. 14. The points indicated by the circles represent the nonlinear STAGS runs. In this case the use of increments in axial displacement instead of increments in axial load makes it possible to get converged solutions on the other side of the limit point, that is on the decreasing branch of the load-displacement curve. By definition the axial load at the limit point corresponds to the collapse load $\rho_s = 0.597$. The load parameter ρ has been here nondimensionalized by the perfect shell buckling load, which for the shell XS-1 is -357.3 N/cm ($= -204.0$ LB/IN) for the C-4 boundary condition[3]. The Extended Analysis[20] results are given by the solid curve. Its limit point occurs at $\rho_s = 0.616$, which is once again very close to the value obtained by STAGS.

A comparison of the collapse modes obtained by the two analyses is shown in Fig. 15. It is apparent from Fig. 15a, showing the axial variation of the radial displacement at $\theta = 13.85^o$, that if the comparison is made at equal maximum amplitudes then the STAGS solution, indicated by the circles, and the Extended Analysis solution[20], indicated by the solid line, are identical to within plotting accuracy. However, for the circumferential variation of the radial displacement at $x = L/2$, shown in Fig. 15b, minor differences will remain also then. Summarizing one can state that also in this case the agreement between the two solutions is remarkably good.

With these results the correctness of the general imperfection subroutine WIMP and the modeling of the C-4 boundary conditions, by applying axial displacements at one end while holding the other end fixed, has been established.

5. Collapse analysis with measured initial imperfections

Now that a method has been found to model the experimental (C-4) boundary conditions and the general imperfection subroutine WIMP is available, the actual imperfections of the stringer stiffened shell AS-2 can be modeled and a collapse analysis carried out using STAGS. This is not as simple a task as might be imagined. To begin with, it is not practical to model the whole shell due to the large number of mesh points required. This requirement arises from the fact that it appears reasonable that the imperfect shell will collapse with a predominant circumferential wave form near that of the perfect shell (14 full waves). Using a criterion of 9 mesh points per half wave, the number of points in the circumferential direction would be approximately 250. Also one needs at least 41 points in the axial direction, according to the convergence studies reported[14]. Thus the number of unknows will be exceedingly large (~ 34000) and the band width of the stiffness matrix too high (~ 340). Because of this nonlinear iterations cannot

be carried out in a reasonable amount of time. It is, therefore, imperative that the shell be subdivided in some appropriate manner.

From a look at the measured initial imperfections (Fig. 3) it is not clear where the appropriate subdivisions should be made. This means that an indefinite number of STAGS runs would be necessary in order to establish, by some process of elimination, the degree of refinement that is necessary to model adequately the effects of the measured initial imperfections. Since the computer funds available for this study were limited, it was decided to use the initial STAGS runs to validate the results obtained by the Multimode Analysis[3] corrected for the effect of the boundary conditions with the formula proposed in Reference [20]. In case that positive correlation between the approximate Multimode Analysis results and the rigorous STAGS solutions is possible, then obviously the above mentioned process of elimination in search of an adequate imperfection model can be run with the much cheaper Multimode Analysis[3]. Once the final model has been established then it can be validated by a single of the more expensive STAGS runs.

5.1. The 7-mode imperfection model

If one chooses the following 7-mode imperfection model

$$\frac{\bar{W}}{t} = 0.0061\cos 2\bar{x} - (0.5072\cos 2\bar{y} + 0.0801\cos 9\bar{y} + 0.0704\cos 10\bar{y} + 0.0626\cos 11\bar{y} + 0.0320\cos 19\bar{y} + 0.0283\cos 21\bar{y})\sin \bar{x} \qquad (29)$$

which is symmetric in the axial direction about the center of the shell, then only half of the shell length needs to be modeled. However, the imperfection model includes modes with both even and odd numbered circumferential waves. This implies that in order to be able to use symmetry conditions at $\theta = 0$ and $\theta = \Delta\theta$, half the shell perimeter must be modeled ($\Delta\theta = 180^{\circ}$). Based on the results of convergence studies[14] this leads to the use of a discrete model consisting of 21 x 131 mesh points. The amplitudes of the asymmetric modes are taken as negative in order to satisfy the favorable coupling conditions[14], which require that at $x = L/2$ and θ (= y/R) = 0 both the axisymmetric and the asymmetric modes must point inward.

In Figure 16 the maximum displacement is plotted as a function of the axial load. Here the maximum displacement is the radial displacement W at $x = L/2$ and $\theta = 0$. The results of the nonlinear STAGS runs are indicated by circles. Above the last point the determinant of the stiffness matrix changes sign indicating the occurrence of an instability. The axial load corresponding to the last converged solution is the collapse load $\rho_s = 0.829$. The load parameter ρ has been nondimensionalized by -320.8 N/cm (= -183.2 LB/IN), which is the buckling load for the perfect shell AS-2 using membrane prebuckling and C-4 boundary conditions[3]. The results of the corresponding Multimode Analysis [3] are given by the solid curve. Its limit point occurs at $\rho_s = 0.825$, which agrees just about exactly with the value obtained by STAGS-A. Further, as can be seen from Figures 17 and 18, the shapes of the radial displacements at the center of the shell (at $x = L/2$) plotted as a function of the circumferential angle θ are very similar for the two methods. Their amplitudes are, however, different by about a factor of 2. This difference is due to the fact that the STAGS-A runs use C-4 boundary conditions, whereas the Multimode Analysis satisfies approximately SS-3 boundary conditions. As is known, under otherwise identical conditions, the maximum radial displacements are for SS-3 boundary conditions by about a factor of two bigger than for C-4 boundary conditions.

Whereas by proper modeling it was possible to achieve excellent agreement between the predictions of the approximate Multimode Analysis and the rigorous STAGS-A solution, still the predicted buckling load of $N_S = (0.83)(-320.8) = -266.3$ N/cm (= -152.1 LB/IN) is about 18% higher than the experimental buckling load of $N_{EXP} = -226.4$ N/cm (= -129.3 LB/IN)[8]. As discussed earlier part of the disagreement might be caused by the difference between the experimental and the idealized (C-4) boundary conditions. On the other hand our numerical study indicates that, if one assumes that by casting the shell ends into Cerrolow a rather stiff connection between the shell wall and the end rings is produced, then the C-4 idealization of the experimental boundary conditions is certainly accurate.

Another explanation for the 18% difference between the predicted and the experimental buckling load may lie in the fact that the imperfection models used up to now do not include enough of the significant imperfection components. Thus further attempts should be made trying to model the measured initial imperfections more accurately. In Reference [14] it was shown that the inclusion of 30 properly chosen initial imperfection harmonics resulted in a buckling load of

$$N_{S_{C-4}} = \rho_s N_{M_{C-4}} = (0.760)(-320.8) = -243.8 \text{ N/cm} = (0.760)(-183.2) = -139.2 \text{ LB/IN} \qquad (30)$$

which is only slightly higher than the experimental buckling load of shell AS-2 of $N_{EXP} = -226.4$ N/cm (= -129.3 LB/IN). This result shows that it is possible to find imperfection representations that will predict the experimental buckling loads quite accurately.

6. Conclusions

This investigation has shown that when for the stringer stiffened shell AS-2 the experimentally determined initial imperfection amplitudes are used, the analysis based on simplified imperfection models all predict "knock-down" factors only slightly less than one. Thus neither a single axisymmetrix imperfection, not an asymmetric imperfection which is affine to the lowest classical buckling mode, nor the so-called 2-Mode Solution consisting of one axisymmetric and one asymmetric mode will predict buckling loads anywhere close to the experimental buckling load if the measured initial amplitudes are used.

The excellent agreement between the properly nondimensionalized Multimode result and the rigorous STAGS solution with all the favorable coupling conditions satisfied suggests the following approach to calculate the appropriate "knock-down" factors based on measured or predicted initial

imperfection distributions. Initially the relatively inexpensive Multimode Analysis should be used to establish by judicious choice of the imperfection and response modes the appropriate initial imperfection model, that will adequately represent the effect of the measured or predicted initial imperfections. Next the effect of the appropriate boundary conditions is included by the use of the proper normalizing factor as described in Reference [20]. At the end the predictions are verified by a single STAGS-run using the imperfection model arrived at by the last Multimode Analysis run.

Finally it will also be necessary to carry out similar correlation studies with the externally ring stiffened shells[8] and the isotropic shells[5] tested at Caltech. For these shells the shapes of the buckling modes are strongly influenced by the type of prebuckling analyses employed, which is not so for the stringer stiffened shell AS-2 used in this investigation. This may affect the correlation between the results obtained by the Multimode Analysis and by STAGS runs.

References

1. Weller, T. and Singer, J.: "Experimental Studies on Buckling of 7075-T6 Aluminum Alloy Integrally Stringer-Stiffened Shells", TAE Rept. 135, Oct. 1971, Technion Research and Development Foundation, Haifa, Israel.
2. Singer, J. and Rosen, A.: "The Influence of Boundary Conditions on the Buckling of Stiffened Cylindrical Shells", Proceedings IUTAM Symposium on Buckling of Structures, Springer Verlag, Heidelberg, 1976, pp. 227-250.
3. Arbocz, J. and Babcock, C.D., Jr.: "Prediction of Buckling Loads Based on Experimentally Measured Initial Imperfections", Proceedings IUTAM Symposium on Buckling of Structures, Springer Verlag, Heidelberg, 1976, pp. 291-311.
4. Hutchinson, J.W. and Amazigo, J.C.: "Imperfection Sensitivity of Eccentrically Stiffened Cylindrical Shells", AIAA Journal, Vol. 5, No. 3, March 1967, pp. 392-401.
5. Arbocz, J. and Babcock, C.D., Jr.: "The Effect of General Imperfections on the Buckling of Cylindrical Shells", Journal of Applied Mechanics, Vol. 36, No. 1, March 1969, pp. 28-38.
6. Arbocz, J.: "The Effect of Initial Imperfections on Shell Stability", Thin Shell Structures, Theory, Experiment and Design, (Y.C. Fung and E.E. Sechler eds.), Prentice-Hall, Englewood Cliffs, N.J., 1974.
7. Almroth, B.O., Brogan, F.A., Miller, E., Zele, F. and Peterson, H.T.: "Collapse Analysis for Shell of General Shape. II. User's Manual for the STAGS-A Computer Code", Air Force Flight Dynamics Lab., Wright Patterson AFB, AFFDL-TR-71-8, March 1973.
8. Singer, J., Arbocz, J. and Babcock, C.D., Jr.: "Buckling of Imperfect Stiffened Cylindrical Shells under Axial Compression", AIAA Journal, Vol. 9, No. 1, Jan. 1971, pp. 68-75.
9. Donnell, L.M. and Wan, C.C.: "Effect of Imperfections on Buckling of Thin Cylinders and Columns under Axial Compression", Journal of Applied Mechanics, Vol. 17, No. 1, March 1950, pp. 73-83.
10. Koiter, W.T.: "On the Stability of Elastic Equilibrium", Ph.D. Thesis, in Dutch, Techn. Univ. Delft, Netherlands. H.T. Paris, Amsterdam. English translation issued as NASA TT F-10, 833 p., 1967.
11. Koiter, W.T.: "The Effect of Axisymmetric Imperfections on the Buckling of Cylindrical Shells under Axial Compression", Koninkl. Ned. Akad. Wetenschap. Proc. B.66, 1963, pp. 265-279.
12. Thurston, G.A. and Freeland, M.A.: "Buckling of Imperfect Cylinders Under Axial Compression", NASA CR-541, July 1966.
13. Geier, B.: "Das Beulverhalten Versteifter Zylinderschalen. Teil 1, Differential-Gleichungen", Z. Flugwiss., Vol. 14, July 1966, pp. 306-323.
14. Arbocz, J. and Babcock, C.D., Jr.: "Utilization of STAGS to Determine Knockdown Factors from Measured Initial Imperfections", Report LR-275, Delft University of Technology, The Netherlands, November 1978.
15. Budiansky, B. and Hutchinson, J.W.: "Dynamic Buckling of Imperfection Sensitive Structures", Proceedings XI. Intern. Congr. Appl. Mech., Springer Verlag, Berlin, 1964, pp. 636-651.
16. Hutchinson, J.W.: "Axial Buckling of Pressurized Imperfect Cylindrical Shells", AIAA Journal, Vol. 3, No. 8, Aug. 1965, pp. 1461-1466.
17. Arbocz, J. and Sechler, E.E.: "On the Buckling of Axially Compressed Imperfect Cylindrical Shells", Journal of Applied Mechanics, Vol. 14, No. 3, Sept. 1974, pp. 737-743.
18. Babcock, C.D., Jr.: "Experiments in Shell Buckling", Thin Shell Structures, Theory, Experiment and Design, (Y.C. Fung and E.E. Sechler, eds.), Prentice-Hall, Englewood Cliffs, N.J., 1974.
19. Arbocz, J. and Babcock, C.D., Jr.: "A Multi-Mode Analysis for Calculating Buckling Loads of Imperfect Cylindrical Shells", GALCIT Report SM74-4, California Institute of Technology, Pasadena, June 1974.
20. Arbocz, J. and Sechler, E.E.: "On the Buckling of Stiffened Imperfect Cylindrical Shells", AIAA Journal, Vol. 14, No. 11, Nov. 1976, pp. 1611-1617.
21. Bushnell, D.: "Stress, Stability, and Vibration of Complex, Branched Shells of Revolution: Analysis and User's Manual for BOSOR-4", NASA CR-2116, Oct. 1972.
22. Cohen, G.A.: "User Document for Computer Programs for Ring-Stiffened Shells of Revolution", NASA CR-2086, March 1973.
23. Singer, J. and Rosen, A.: "The Influence of Boundary Conditions on the Buckling of Stiffened Cylindrical Shells", T.A.E. Rept. 213, June 1974, Technion Research and Development Foundation, Haifa, Israel.
24. Rosen, A. and Singer, J.: "Vibration of Axially Loaded Stiffened Cylindrical Shells with Elastic Restraints", Int. Journal Solids Structures, Vol. 12, No. 8, Aug. 1976, pp. 577-588.
25. Babcock, C.D., Jr.: "Utilization of STAGS to determine knockdown factors from Measured Initial Imperfections", Status Report ## 1 - NASA Research Grant NsG1005, GALCIT, California Institute of Technology, Pasadena, Feb. 1975.

Table 1. Geometric properties of shell AS-2.

t	$= 1.96596 \times 10^{-2}$ cm	(= 0.00774	IN)
L	$= 13.97$ cm	(= 5.50	IN)
R	$= 10.16$ cm	(= 4.00	IN)
d_1	$= 8.03402 \times 10^{-1}$ cm	(= 0.3163	IN)
e_1	$= 3.36804 \times 10^{-2}$ cm	(= 0.01326	IN)
A_1	$= 7.98708 \times 10^{-3}$ cm^2	(= 0.1238×10^{-2}	IN^2)
I_{11}	$= 1.50384 \times 10^{-6}$ cm^4	(= 0.3613×10^{-7}	IN^4)
I_{t_1}	$= 4.94483 \times 10^{-6}$ cm^4	(= 0.1188×10^{-6}	IN^4)
E	$= 6.89472 \times 10^{6}$ N/cm^2	(= 10×10^{6}	PSI)
ν	$= 0.3$		

Table 4. Summary of the imperfection model parameters for shell AS-2.

$\bar{X}_A = 0.0072$, $q = 0.247$
$\bar{X} = 1.1873$, $r = 1.123$, $s = 1.227$

Table 5. Buckling loads calculated by the Multi-Mode Analysis [3].

No. of modes	ρ_s
2-modes (2,0) + (1,10)	= 0.904
4-modes (2,0) + (1,10) + (9,10) + (10,0)	= 0.903
7-modes (2,0) + (1,2) + (1,9) + (1,10) + (1,11) + + (1,19) + (1,21)	= 0.825
14-modes (2,0) + (1,2) + (1,9) + (1,10) + (1,11) + + (1,19) + (1,21) + (9,2) + (9,9) + + (9,10) + (9,11) + (9,19) + (9,21) + + (10,0)	= 0.824

Table 6. Definition of the boundary conditions.

SS-1 : $N_x = N_{xy} = w = M_x = 0$
SS-2 : $u = N_{xy} = w = M_x = 0$
SS-3 : $N_x = v = w = M_x = 0$
SS-4 : $u = v = w = M_x = 0$

C-1 : $N_x = N_{xy} = w = w_{,x} = 0$
C-2 : $u = N_{xy} = w = w_{,x} = 0$
C-3 : $N_x = v = w = w_{,x} = 0$
C-4 : $u = v = w = w_{,x} = 0$

$A_{k\ell}$ components - $\cos \frac{k\pi x}{L} \cos \frac{\ell y}{R}$

ℓ =	0	1	2	3	4	5	6	7	8	9	10	11	12	13	14
k = 0	0.0	0.0	0.247	0.167	0.180	-0.012	-0.026	0.025	-0.046	0.058	-0.026	0.004	0.028	-0.021	0.023
k = 1	0.001	0.0	0.256	-0.016	0.073	-0.020	-0.013	-0.022	-0.017	0.001	-0.022	-0.002	-0.008	-0.003	0.0
k = 2	0.005	-0.002	-0.005	0.003	-0.008	0.012	0.010	-0.020	0.019	-0.014	0.008	0.003	-0.006	0.008	-0.007
k = 3	0.0	0.001	0.027	-0.002	0.006	-0.004	-0.001	0.0	-0.002	0.001	0.0	0.0	-0.002	0.0	-0.003
k = 4	0.004	0.0	-0.001	-0.001	-0.003	0.002	0.002	-0.003	0.004	-0.006	0.005	0.0	-0.002	0.002	0.0
k = 5	-0.003	0.0	0.012	-0.002	0.005	0.0	0.0	-0.001	0.0	0.0	0.0	0.0	0.0	0.0	0.0
k = 6	0.0	0.0	-0.001	-0.001	-0.002	0.002	0.001	-0.001	0.002	-0.003	0.0	0.002	-0.002	0.001	0.0
k = 7	0.002	0.001	0.006	-0.001	0.001	0.0	0.0	0.0	0.0	0.0	0.0	0.0	-0.001	0.0	0.0
k = 8	-0.002	0.0	0.0	0.0	-0.002	0.002	0.0	0.0	0.0	-0.002	0.0	0.001	-0.001	0.0	0.0
k = 9	0.0	0.0	0.003	0.0	0.0	0.0	0.0	0.0	0.0	-0.001	0.0	0.0	0.0	0.0	0.0
k = 10	-0.001	0.0	0.0	0.0	-0.002	0.0	0.0	0.0	0.0	-0.002	0.0	0.0	0.0	0.0	0.0

$B_{k\ell}$ components - $\cos \frac{k\pi x}{L} \sin \frac{\ell y}{R}$

ℓ =	0	1	2	3	4	5	6	7	8	9	10	11	12	13	14
k = 0	-	0.0	0.095	-0.023	-0.003	0.032	-0.071	-0.029	-0.003	-0.026	0.029	-0.039	0.018	0.003	-0.010
k = 1	-	0.0	-0.092	-0.094	0.004	-0.017	-0.005	-0.013	0.0	0.0	0.010	-0.006	0.003	0.003	0.0
k = 2	-	0.003	0.003	-0.001	0.003	-0.013	0.009	0.003	-0.005	0.009	-0.007	0.012	-0.011	0.002	0.003
k = 3	-	0.0	-0.010	-0.010	-0.001	-0.003	0.0	0.0	0.003	0.0	0.0	0.002	0.0	0.001	0.0
k = 4	-	0.0	0.001	0.0	-0.001	-0.005	0.003	0.001	0.002	0.001	-0.001	0.002	-0.002	0.0	0.0
k = 5	-	0.0	-0.002	-0.003	0.0	0.0	0.0	0.0	-0.001	0.0	0.0	0.003	0.0	0.0	0.002
k = 6	-	0.0	0.001	0.0	0.0	-0.002	0.002	0.0	0.0	0.0	-0.001	0.002	0.0	0.0	0.0
k = 7	-	0.0	0.0	-0.003	-0.002	0.0	0.0	0.0	0.0	0.0	0.0	0.0	0.0	0.0	0.0
k = 8	-	0.001	0.0	0.0	0.0	-0.001	0.0	0.0	0.0	0.0	0.0	0.0	0.0	0.0	0.0
k = 9	-	0.0	0.0	-0.001	0.0	0.0	0.0	0.0	0.0	0.0	0.0	0.0	0.0	0.0	0.0
k = 10	-	0.002	0.0	0.0	0.0	-0.001	0.0	0.001	0.0	0.0	0.0	0.0	0.0	0.0	0.0

Table 2. Fourier coefficients of the half-wave cosine representation.

$C_{k\ell}$ components - $\sin \frac{k\pi x}{L} \cos \frac{\ell y}{R}$

ℓ =	0	1	2	3	4	5	6	7	8	9	10	11	12	13	14
k = 1	-0.001	0.002	0.316	0.211	0.232	-0.021	-0.038	0.040	-0.066	0.080	-0.037	0.003	0.038	-0.031	0.033
k = 2	0.001	-0.002	0.230	-0.012	0.058	-0.015	-0.010	-0.018	-0.013	0.0	-0.018	-0.001	-0.006	-0.002	0.002
k = 3	0.002	-0.002	0.100	0.072	0.071	0.002	-0.005	-0.003	-0.007	0.018	-0.008	0.003	0.008	-0.004	0.005
k = 4	0.002	0.0	0.095	-0.005	0.025	-0.009	-0.005	-0.007	-0.006	0.002	-0.007	0.0	-0.003	-0.002	-0.002
k = 5	0.005	0.0	0.058	0.041	0.041	0.0	-0.003	-0.001	-0.004	0.008	-0.002	0.0	0.005	-0.002	0.004
k = 6	-0.003	0.0	0.063	-0.004	0.019	-0.004	-0.003	-0.006	-0.004	0.0	-0.005	-0.001	-0.002	0.0	0.0
k = 7	0.003	0.0	0.038	0.027	0.027	0.0	-0.002	0.0	-0.002	0.005	-0.002	0.002	0.003	-0.001	0.002
k = 8	0.0	0.0	0.044	-0.003	0.013	-0.004	-0.002	-0.004	-0.003	0.001	-0.003	0.0	-0.002	0.0	0.0
k = 9	0.001	0.0	0.027	0.020	0.019	0.001	0.0	0.0	-0.002	0.004	-0.002	0.002	0.001	0.0	0.002
k = 10	0.0	0.0	0.033	-0.001	0.010	-0.002	-0.002	-0.002	-0.002	0.0	-0.003	0.0	-0.002	0.0	0.0

$D_{k\ell}$ components - $\sin \frac{k\pi x}{L} \sin \frac{\ell y}{R}$

ℓ =	0	1	2	3	4	5	6	7	8	9	10	11	12	13	14
k = 1	-	-0.002	0.119	-0.029	-0.005	0.046	-0.094	-0.039	-0.001	-0.037	0.040	-0.055	0.028	0.003	-0.013
k = 2	-	-0.001	-0.072	-0.074	0.004	-0.013	-0.004	-0.012	-0.002	0.0	0.008	-0.007	0.002	0.002	-0.001
k = 3	-	0.0	0.041	-0.010	0.002	0.007	-0.025	-0.011	-0.006	-0.005	0.008	-0.009	0.0	0.003	-0.002
k = 4	-	0.0	-0.036	-0.036	0.0	-0.007	0.0	-0.004	0.002	0.0	0.004	-0.002	0.002	0.002	-0.001
k = 5	-	0.0	0.024	-0.006	0.0	0.002	-0.014	-0.006	0.0	-0.003	0.005	-0.006	0.0	0.001	-0.002
k = 6	-	0.0	-0.022	-0.022	0.002	-0.004	-0.001	-0.003	-0.001	0.0	0.002	0.0	0.002	0.001	0.0
k = 7	-	0.0	0.017	-0.003	0.0	0.001	-0.008	-0.005	-0.001	-0.002	0.003	-0.003	0.0	0.0	0.0
k = 8	-	0.0	-0.015	-0.016	-0.001	-0.003	0.0	-0.001	0.0	0.0	0.001	0.0	0.0	0.0	0.0
k = 9	-	0.0	0.013	-0.002	0.0	0.0	-0.006	-0.004	0.0	-0.002	0.002	-0.002	0.0	0.0	-0.001
k = 10	-	0.0	-0.010	-0.012	0.0	0.0	0.0	0.0	0.0	0.0	0.002	0.0	0.0	0.0	0.0

Table 3. Fourier coefficients of the half-wave sine representation.

Fig. 1. Comparison of theory and experiment for stringer stiffened shells under axial compression[1].

Fig. 2. Geometry of the stringer stiffened shell AS-2[8].

Fig. 3. Measured initial shape of the stringer stiffened shell AS-2[8].

Fig. 4. Buckling loads from linear theory for stringer stiffened shell AS-2 (Boundary conditions: $N_x = v = w = M_x = 0$).

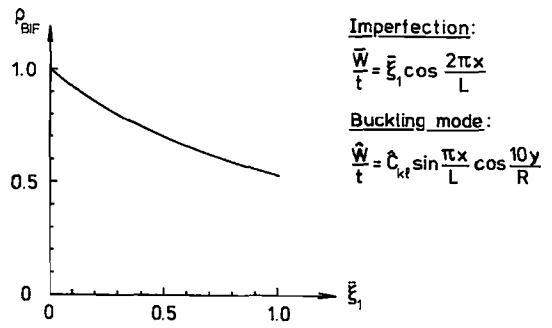

Fig. 5. Imperfection sensitivity for axisymmetric imperfection only (Shell AS-2).

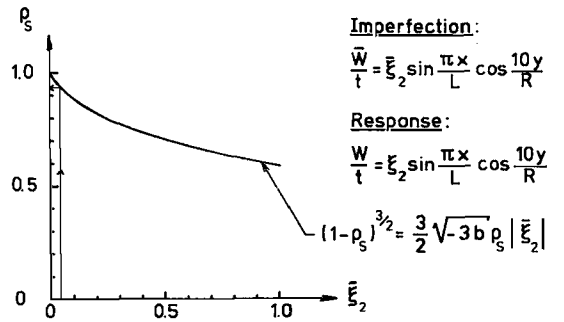

Fig. 6. Imperfection sensitivity for asymmetric imperfection only (Shell AS-2, b = -0.0308).

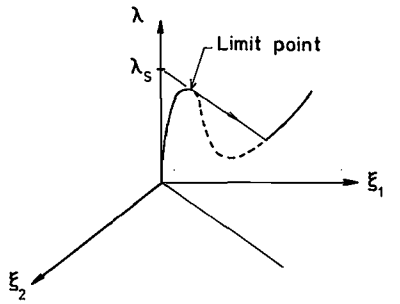

Fig. 7. Equilibrium configurations for an imperfect shell.

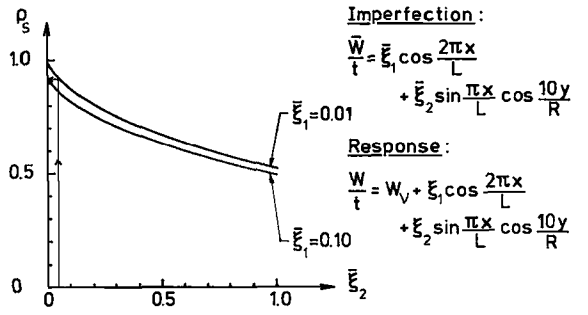

Fig. 8. Imperfection sensitivity for 1-axisymmetric and 1-asymmetric imperfection (Shell AS-2).

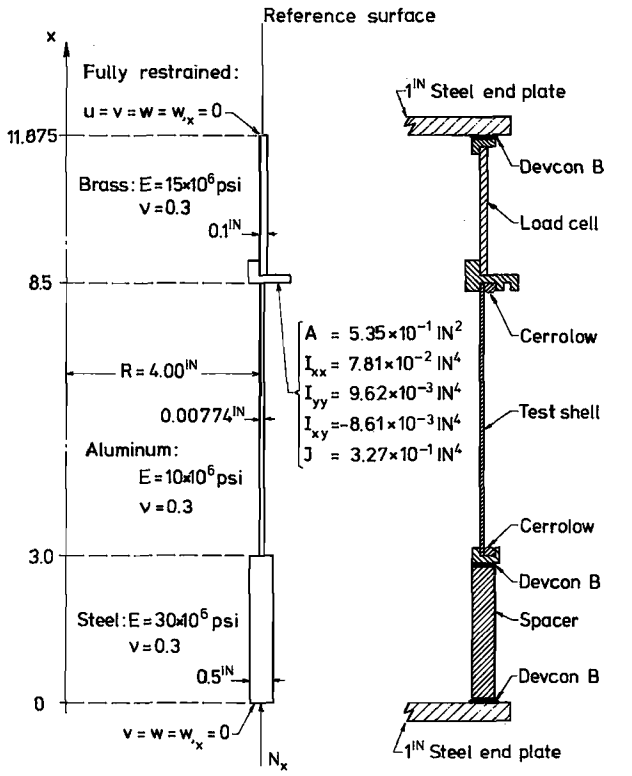

Fig. 9. Test set-up and corresponding computer model.

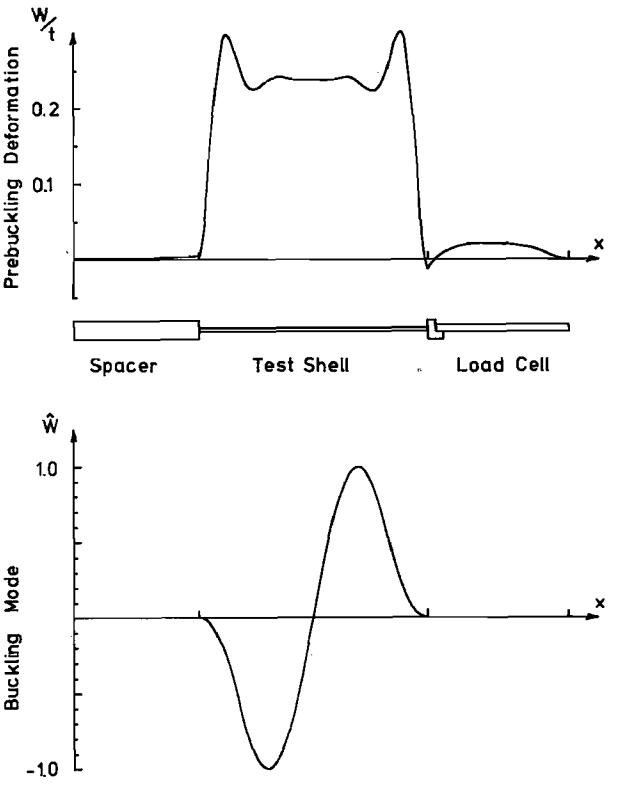

Fig. 10. Prebuckling deformation and buckling mode for Shell AS-2 (Experimental boundary conditions).

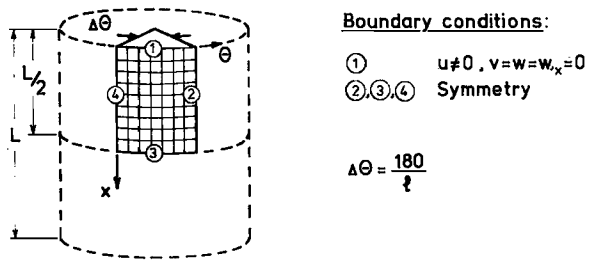

Fig. 11. Shell segment used for collapse analysis with idealized imperfections (Shell XS-1).

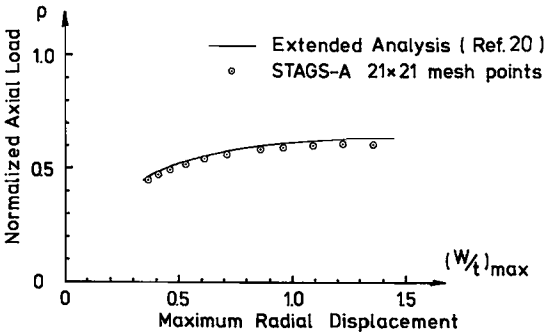

Fig. 12. Comparison of Extended Analysis and STAGS-A (Shell XS-1; Boundary conditions: $N_x = v = w = w_{,x} = 0$; $\ell = 11$).

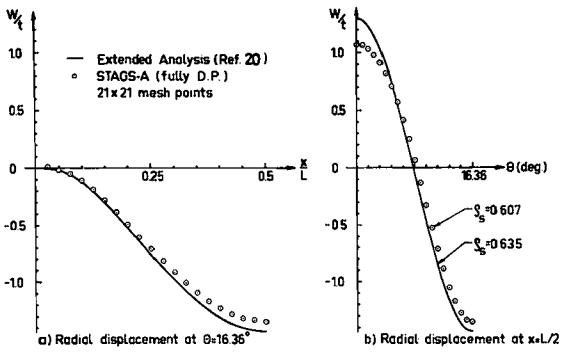

Fig. 13. Radial displacement of Extended Analysis and STAGS-A (Shell XS-1; Boundary conditions: $N_x = v = w = M_x = 0$; $\ell = 11$).

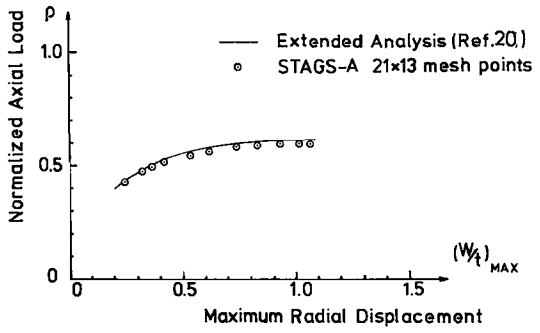

Fig. 14. Comparison of Extended Analysis and STAGS-A (Shell XS-1, Boundary conditions: $u = v = w = w_{,x} = 0$; $\ell = 13$).

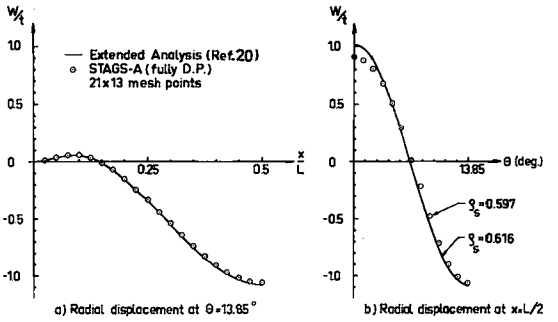

Fig. 15. Radial displacements of Extended Analysis and STAGS-A (Shell XS-1, Boundary conditions: $u = v = w = w_{,x} = 0$; $\ell = 13$).

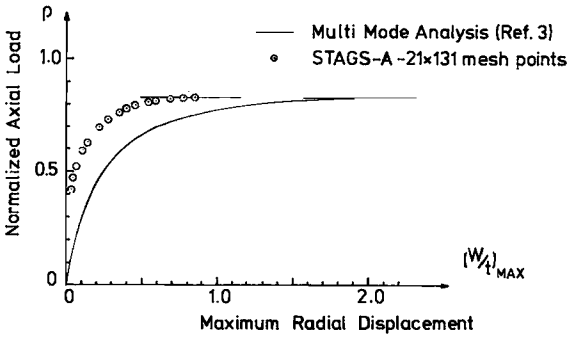

Fig. 16. Comparison of Multi Mode Analysis and STAGS-A (Shell AS-2, 7-Modes Imperfection Model).

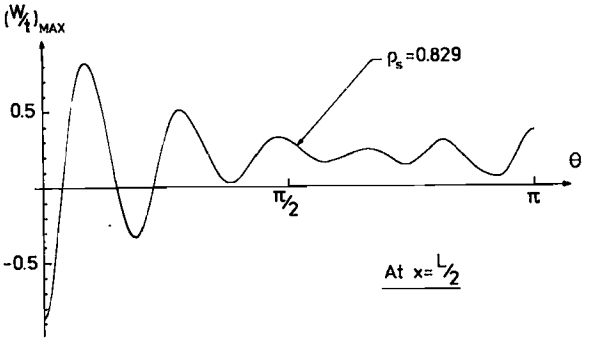

Fig. 17. Radial displacement at the limit point by STAGS-A (Shell AS-2, 7-Modes Imperfection Model).

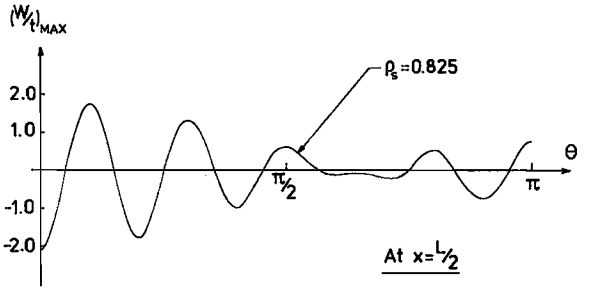

Fig. 18. Radial displacement at the limit point by Multi Mode Analysis[3] (Shell AS-2, 7-Modes Imperfection Model).